1997

Preparation of Nd-doped BaCeO3 Proton-Conducting Ceramics by Homogeneous Oxalate Coprecipitation

Fanglin Chen
University of South Carolina - Columbia, fchen@sc.edu

Ping Wang
University of Science and Technology of China

O. Toft Sorensen

Guangyao Meng
University of Science and Technology of China

Dingkum Peng
University of Science and Technology of China

Publication Info

Journal of Materials Chemistry, Volume 7, Issue 8, 1997, pages 1533-1539.

Publisher's Version: http://dx.doi.org/10.1039/A608289K
DOI: 10.1039/A608289K

Preparation of Nd-doped $BaCeO_3$ proton-conducting ceramics by homogeneous oxalate coprecipitation

Fanglin Chen,[a] Ping Wang,[a] O. Toft Sørensen,[b] Guangyao Meng[a] and Dingkun Peng[a]

[a]*Department of Materials Science and Engineering, University of Science and Technology of China, Hefei, Anhui 230026, P.R. China*

[b]*Materials Department, Risø National Laboratory, DK-4000 Roskilde, Denmark*

Nd-doped $BaCeO_3$ have been obtained from homogeneous coprecipitated oxalates when calcined at temperatures $T \geqslant 1000\,^{\circ}C$. Ball-milling of the calcined powders well disperses the agglomerates and consequently has a beneficial effect in the densification process. The calcination temperature has a major influence on the sintering process and powders calcined at 1100 °C possess good sinterabilities. The pressure applied to press the green pellets has no apparent influence on the sintered density at sintering temperatures of $T \geqslant 1400\,^{\circ}C$. By controlling the processing variables it was possible to obtain near fully dense Nd-doped $BaCeO_3$ ceramics with homogeneous microstructure at a sintering temperature as low as 1300 °C. Electrical conductivities of the sintered samples were measured in dry and moist air and in hydrogen in the temperature range 500–800 °C using complex impedance techniques. Much higher proton conductivity was obtained in this work compared with previously reported values, in which the samples were prepared from traditional ceramic methods.

$BaCeO_3$ and $SrCeO_3$ doped with rare-earth oxides such as Nd_2O_3 are known to exhibit significant protonic conduction in atmospheres containing hydrogen or water vapour at elevated temperatures.[1] Their ability to conduct protons makes them potential candidates for applications in solid oxide fuel cells, hydrogen or steam sensors and membrane reactors,[2–5] although their stability at cell operating temperatures with high steam partial pressures, *i.e.* higher level of fuel utilisation, is still open to question.[6]

These materials are usually formed by a conventional ceramic process consisting of calcining mixtures of the respective oxides and carbonates at temperatures $\geqslant 1200\,^{\circ}C$ followed by sintering the powder compacts at temperatures of 1400–1600 °C.[7] The solid-state reaction is a diffusion controlled process which requires intimacy of reacting species and an uniform distribution of each species to obtain a completely reacted and uniform product. Since the starting materials generally have a large particle size, this approach frequently needs repeated mixing and extended heating at high temperature in order to generate a homogeneous and single phase material.[8] The mechanical mixing process will very likely introduce contaminants from abrasive materials.[9] Moreover, prolonged calcination promotes crystallite growth which is undesirable in the fabrication of dense fine-grained ceramics which undoubtedly possess better electrical properties. In order to overcome all these disadvantages, precursors generated by sol–gel preparations or coprecipitation of metal ions may be a promising alternative. The principal advantages of starting from solution are better homogeneity and improved reactivity. The necessary solid-state reactions proceed more rapidly and at lower temperatures. As a consequence, the desired product can be obtained with a smaller particle size and greater reactivity.

To date, only a few wet chemical processes were attempted to prepare such materials. An electrostatic spray pyrolysis (ESP) method was applied by Kelder *et al.*,[10] and $BaCeO_3$ thin films were synthesized at 400 °C. The results seemed promising, but some other phases were present in the final product and further investigation should be undertaken. A modified Pechini process using EDTA as a chelating agent was attempted by Agarwal and Liu,[11] and $BaCeO_3$-based thin films were prepared at 750 °C. The oxalate coprecipitation route was employed by Flint and Slade[12] to prepare Ca- and Gd-doped $BaCeO_3$ ceramics. Their results showed that the calcination temperature needed to obtain a single perovskite phase from oxalate coprecipitated powders was $T \geqslant 1000\,^{\circ}C$, several hundred degrees lower than that from a carbonate–oxide mixture ($T > 1250\,^{\circ}C$). However, the work of Flint and Slade concentrated on the electrical properties and the materials preparation route requires further investigation. The main purpose of this work is to prepare Nd-doped $BaCeO_3$ ceramic by the oxalate coprecipitation method, to study the calcining and sintering process, and to evaluate the electrical properties of the sintered samples obtained by this technique.

Experimental

The flow chart for preparing Nd-doped $BaCeO_3$ ceramics is illustrated in Fig. 1. The stoichiometric ratio of $Ba(NO_3)_2$ (Merck), $Ce(NO_3)_3{\cdot}6H_2O$ (Alfa) and $Nd(NO_3)_3{\cdot}6H_2O$ (Aldrich) to yield the composition $BaCe_{0.9}Nd_{0.1}O_{3-\delta}$ were dissolved in deionized water and heated to reflux. Excess hot aqueous ammonium oxalate was added to the nitrate solution with vigorous stirring to effect instantaneous oxalate coprecipitation. The precipitate was stood at room temperature for 10 h to allow crystallization. After filtering, the precipitate was washed with deionized water and then dried in an oven at 110 °C for 24 h. The obtained precipitate powders consist of fine particles of submicrometre size, as illustrated in Fig. 2.

Simultaneous differential thermal analysis and thermogravimetry (DTA–TG) were carried out on the precipitate powders using a thermal analyser (Netzsch STA 429). Samples were heated from 25 to 1400 °C at a heating rate of $2\,^{\circ}C\ min^{-1}$ under dynamic air flow. The powders were calcined in static air for 8 h from 600 to 1200 °C and then were characterized by X-ray powder diffraction (XRD; Philips PW1078). The powders calcined at a temperature of $\geqslant 1000\,^{\circ}C$ were treated in two different ways. One sample was simply ground using an agate mortar and pestle, while the other was ground and subsequently ball-milled in ethanol for 4 h and then dried. The differently treated powders were examined by a laser scattering particle size analyser (Malvern MasterSizer/E) and by scanning electron microscopy (SEM; JEOL JSM-840).

The two differently treated powders were uniaxially pressed

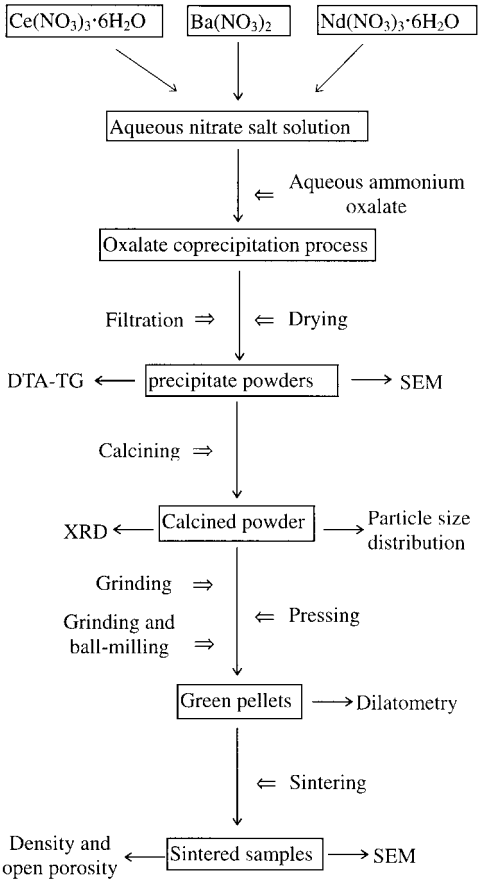

Fig. 1 Flow chart of the experimental procedure

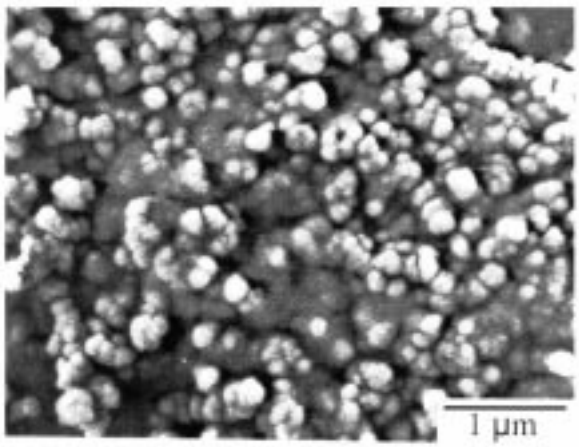

Fig. 2 Scanning electron micrograph of the precipitate powders

into pellets at 100 MPa, without added binder, with a diameter of 10 mm and a thickness of *ca.* 3 mm. The study of the sintering process was performed on the pressed compacts using a dilatometer (Netzsch type 402E). A constant heating rate of 2 °C min^{-1} was adopted and the sintering temperature was 1500 °C. The 1100 °C calcined and ball-milled powders were pressed into pellets using different pressing pressures of 50, 100, 200 and 350 MPa. The green pellets were sintered in air in the temperature range 1200–1400 °C for 10 h or at 1500 °C for 2 h. The bulk density and open porosity of the sintered samples were measured by the Archimedes method using water as the liquid medium. The sintered samples were polished on SiC paper and then thermally etched at a temperature 200 °C lower than the sintering temperature for 2 h. Sintered surfaces, fracture surfaces as well as thermally etched polished surfaces of the sintered samples were examined by SEM.

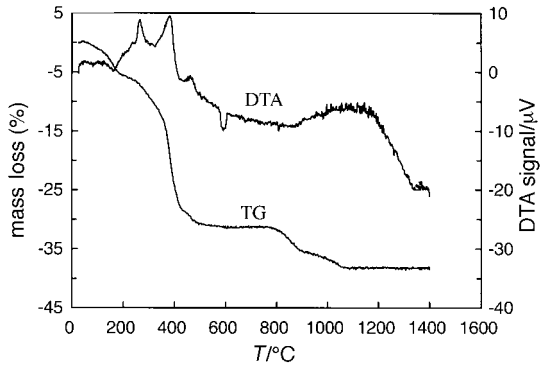

Fig. 3 DTA–TG curve for the oxalate coprecipitated powder

Electrodes were applied to polished pellets sintered at 1300, 1400 and 1500 °C, by painting platinum paste and then baking at 1000 °C. Conductivity was measured by the ac impedance method over the frequency range 12–10^5 Hz using a GenRad 1689 precision RLC digibridge programmed *via* an IBM-compatible computer for data collection and analysis.[13] The set-up of the conductivity measurement was mounted horizontally in an electric-tube furnace with controlled gas flow (gas flow rate = 50 ml min^{-1}). Measurements were conducted in different atmospheres of dry and moist air and in hydrogen in the temperature range 500–800 °C. 'Dry' air was obtained by passing air through anhydrous $CaCl_2$, then through an activated molecular sieve column and finally P_2O_5, whereas 'moist' air was obtained by passage through a water bubbler at 50 °C, which is equivalent to a water vapour partial pressure of 92.51 Torr. Hydrogen gas used in this work was pure hydrogen from a gas cylinder.

Results and Discussion

DTA–TG

DTA–TG was used in analysing the decomposition of the precipitate powders and the formation of $BaCe_{0.9}Nd_{0.1}O_{3-\delta}$ perovskite phase. Fig. 3 shows the DTA–TG result of the precipitate powders in air. At $T < 200$ °C, there is a *ca.* 6% mass loss which is caused by the endothermic removal of the surface and occluded water. In the temperature range 200–500 °C, there is a large mass loss accompanied by three exothermic DTA peaks. In this temperature range, barium and neodymium oxalates decompose into carbonates, whereas cerium oxalate decomposes into cerium oxide. At *ca.* 590 °C, there is a small mass loss accompanied by an endothermic DTA peak, which corresponds to the decomposition of neodymium carbonate. At *ca.* 800 °C, another mass loss starts which is complete at *ca.* 1050 °C. This is ascribed to the thermal decomposition of $BaCO_3$ and the formation of the $BaCe_{0.9}Nd_{0.1}O_{3-\delta}$ perovskite phase, as evidenced by XRD. No apparent mass loss occurs at $T > 1050$ °C, indicating that the decomposition of $BaCO_3$ and the formation of $BaCe_{0.9}Nd_{0.1}O_{3-\delta}$ perovskite phase is complete.

X-Ray powder diffraction

The precipitated powders were heated between 600 and 1200 °C, at 100 °C intervals, for 8 h, and the products were identified by XRD. Only carbonate and oxide were present and no $BaCe_{0.9}Nd_{0.1}O_{3-\delta}$ perovskite phase was formed below 600 °C, as illustrated in Fig. 4. When the temperature was raised to 700 °C, the solid-state reaction between $BaCO_3$, CeO_2 and Nd_2O_3 started, and several diffraction peaks belonging to the $BaCe_{0.9}Nd_{0.1}O_{3-\delta}$ perovskite phase appeared. With increased firing temperature, more perovskite phase formed in the products, with a corresponding decrease in the carbonate and oxide phases. The formation of $BaCe_{0.9}Nd_{0.1}O_{3-\delta}$ was

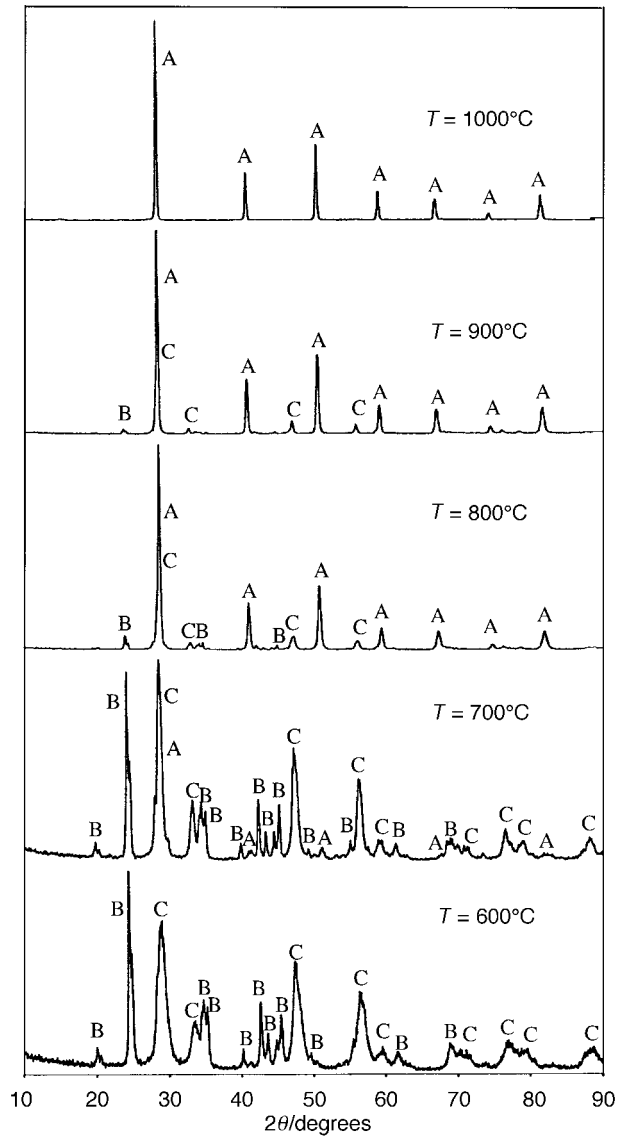

Fig. 4 X-Ray diffraction patterns of the precipitate heated at the temperatures indicated for 8 h. A, B and C indicate diffraction peaks produced from $BaCe_{0.9}Nd_{0.1}O_{3-\delta}$, $BaCO_3$ and CeO_2, respectively.

complete by 1000 °C, and no carbonate and oxide could be detected. As shown in Fig. 2, the precipitate powders consist of homogeneous small particles of submicrometre size. Such highly reactive small particles are ideal for the consequent solid-state reaction to form the $BaCe_{0.9}Nd_{0.1}O_{3-\delta}$ perovskite phase.

Particle size distribution analysis

To ensure the complete formation of $BaCe_{0.9}Nd_{0.1}O_{3-\delta}$, the precipitate was calcined at a temperature of $\geqslant$1000 °C for 8 h. Particle size distribution analysis was performed on the differently treated calcined powders. Similar results were found for powders calcined at different temperatures, and typical particle size distributions of powders calcined at 1100 °C by different treatments are shown in Fig. 5. The results show that powders produced from mortar and pestle grinding have a wide range of particle size distribution and that some agglomerates are present, while those after ball-milling have a narrow range of particle size distribution and consist of very homogeneous particles of submicrometre size and no agglomerates. Therefore, ball-milling of the calcined powders in ethanol effectively disperses the agglomerates so that small particles are dominant in the ball-milled powder. Fig. 6 shows the mean particle size of the calcined powders by different treatments. It can be seen

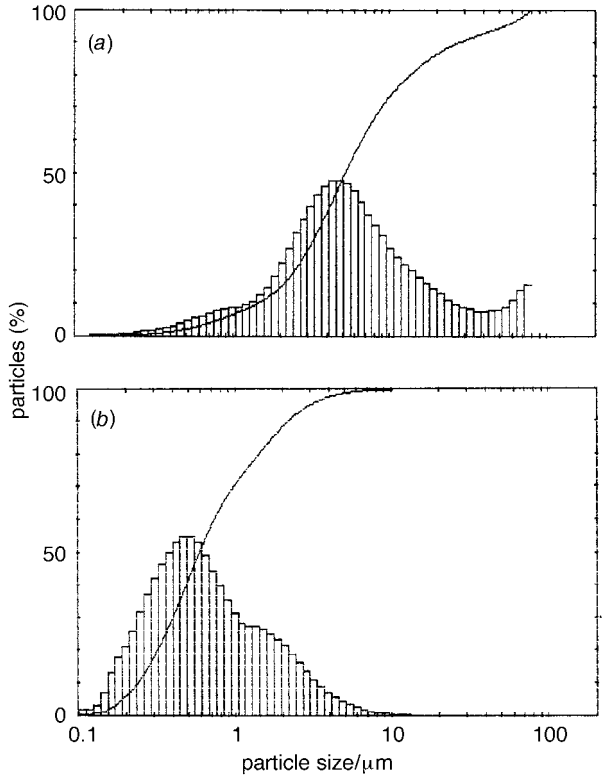

Fig. 5 Particle size distributions of 1100 °C calcined, differently treated powders: (*a*) ground, (*b*) ball-milled in ethanol

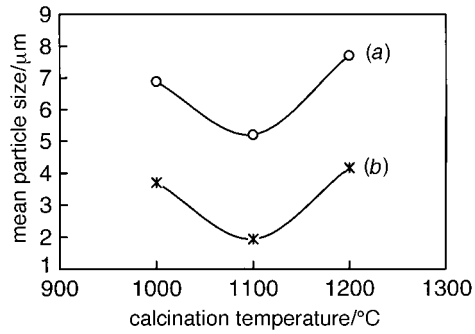

Fig. 6 Mean particle size of the (*a*) ground and (*b*) ball-milled calcined powders

that fine $BaCe_{0.9}Nd_{0.1}O_{3-\delta}$ precursor powders with small particle sizes are produced by the oxalate coprecipitation technique.

Shrinkage curves of the pressed compacts

The shrinkage behaviour of the specimens from differently treated calcined powders was measured using a dilatometer, and results are shown in Fig. 7. The specimens started shrinking at *ca.* 1100 °C. The shrinkage rate of the specimen from the ball-milled powder is comparatively larger than that from the ground powder in the entire temperature range studied, indicating that ball-milling of the calcined powders in ethanol has a favourable effect on the densification process.

Density and open porosity of the sintered samples

The sintered density, as shown in Fig. 8, indicates that the calcination temperature has a major influence on the densification properties. Too low or too high a calcination temperature is unfavourable for the sintering process. Ball-milling of the calcined powders can apparently increase the sintered density. From the open porosity of the sintered samples, Table 1, it can be noted that the sintered samples

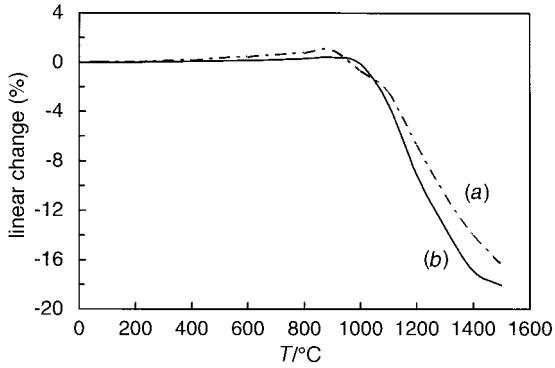

Fig. 7 Shrinkage curves of the compacts from (*a*) ground and (*b*) ball-milled calcined powders

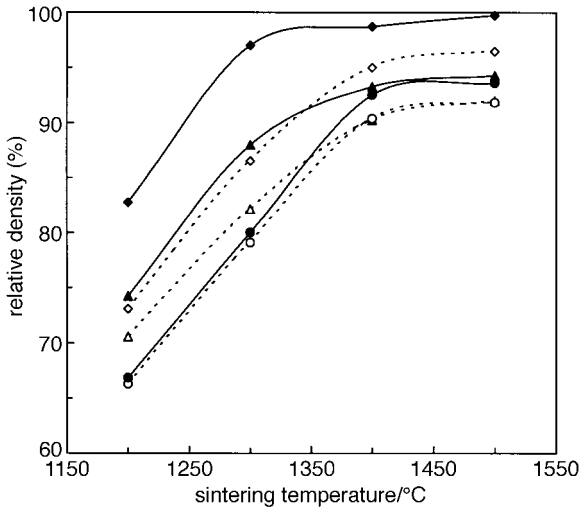

Fig. 8 Sintered density as a function of temperature at the following calcination temperatures: (△, ▲) 1000, (◇, ◆) 1100, (○, ●) 1200 °C. Open symbols: samples of ground powders; filled symbols: samples of ball-milled powders.

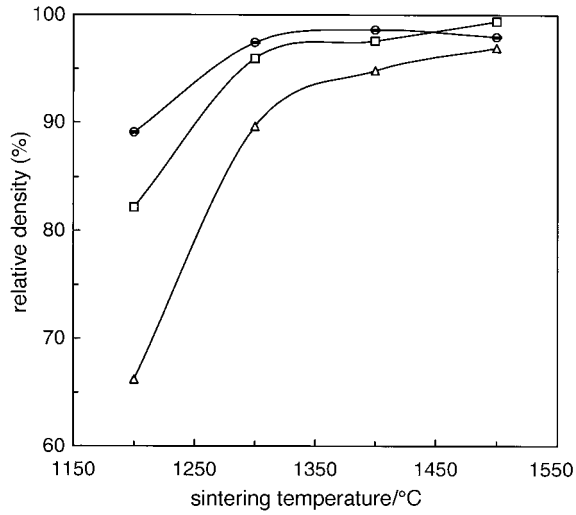

Fig. 9 Effect of pressing pressure on sintered density. $P = 50$ (△), 100 (□), 200 (○), 350 MPa (-).

from ball-milled powders have comparatively less open porosity than those from ground powders, especially at low sintering temperatures. The optimum calcination temperature is 1100 °C, and the sintered samples from this powder have higher density and less open porosity compared with those from powders calcined at other temperatures. This may be a consequence of the smaller mean particle size of powders calcined at 1100 °C, as shown in Fig. 6. Consequently, when

Table 1 Open porosity of the sintered samples[a]

	$T_{calcination}$/°C		
$T_{sintering}$/°C	1000	1100	1200
1200	24.9 (23.9)	24.2 (14.5)	30.2 (29.8)
1300	12.9 (8.8)	10.6 (0.1)	18.8 (15.3)
1400	4.1 (0)	0.2 (0)	0.1 (4.8)
1500	0.1 (0.1)	0 (0.1)	0.2 (3.4)

[a]Values in parentheses denote the open porosity of the sintered samples from ball-milled powders, while the other values are the open porosity of the sintered samples from ground powders.

sintered at a temperature as low as 1300 °C, samples with >97% theoretical density can be obtained by optimizing calcining and sintering conditions. Sintering at 1500 °C gives ceramics with a density >99% of the theoretical value.

Influence of pressing pressure on the sintered density

Fig. 9 shows how the sintered density of the ball-milled samples calcined at 1100 °C is influenced by the pressure applied to press the green pellets. The results show that at low sintering temperatures, the pressing pressure has a strong positive influence on the sintered density. However, at high sintering temperatures, *i.e.*, $T \geqslant 1400$ °C, the pressing pressure has little influence on the sintered density. When sintered at $T \geqslant 1400$ °C, a sintered density >95% of the theoretical value can be obtained even when the pressing pressure is as low as 50 MPa. Moreover, at sintering temperatures of $T \geqslant 1300$ °C, when the pressure exceeds 100 MPa, further increasing the pressure has no apparent influence on the sintered density. As indicated in Fig. 5, ball-milling of $BaCe_{0.9}Nd_{0.1}O_{3-\delta}$ precursor powders in ethanol results in well dispersed fine particles with submicrometre size, and this is favourable for the densification process. Accordingly, the pressing pressure does not play an important role in increasing the sintered density.

Microstructural development

SEM images of the sintered surfaces, fracture surfaces, and thermally etched polished surfaces of the sintered ball-milled samples calcined at 1100 °C and sintered at 1200 °C and above are shown in Fig. 10, 11 and 12. These micrographs illustrate that a rapid densification process takes place as the sintering temperature is increased. Upon sintering at 1200 °C, only a porous microstructure is observed, but at $T \geqslant 1300$ °C, dense, homogeneous microstructures are obtained. Grain growth can be observed with an increase in sintering temperatures. Neither coarsening nor exaggerated grain growth occurred in the sintered samples. No intergranular porosity was observed and all the pores were located at the grain boundaries or at triple points. The facts that a homogeneous microstructure was obtained, that the porosity remained at the grain boundaries and that no exaggerated grain growth was produced were a consequence of the well dispersed $BaCe_{0.9}Nd_{0.1}O_{3-\delta}$ precursor powders produced by the oxalate coprecipitation technique.

Electrical conductivity

Electrical conductivity was evaluated for samples sintered at 1300, 1400 and 1500 °C, in the temperature range 500–800 °C in dry and moist air, and in a hydrogen atmosphere. Similar results were obtained for samples sintered at different temperatures. Fig. 13 shows the Arrhenius plots of the conductivity of Nd-doped $BaCeO_3$ materials observed in this work as well as results reported in the literature. It can be seen that in the temperature range studied in this work, at a given temperature, the conductivity values in hydrogen and in moist air are very close to each other, and are comparatively much larger than that in dry air. The activation energy is 47.6 kJ mol^{-1} in a

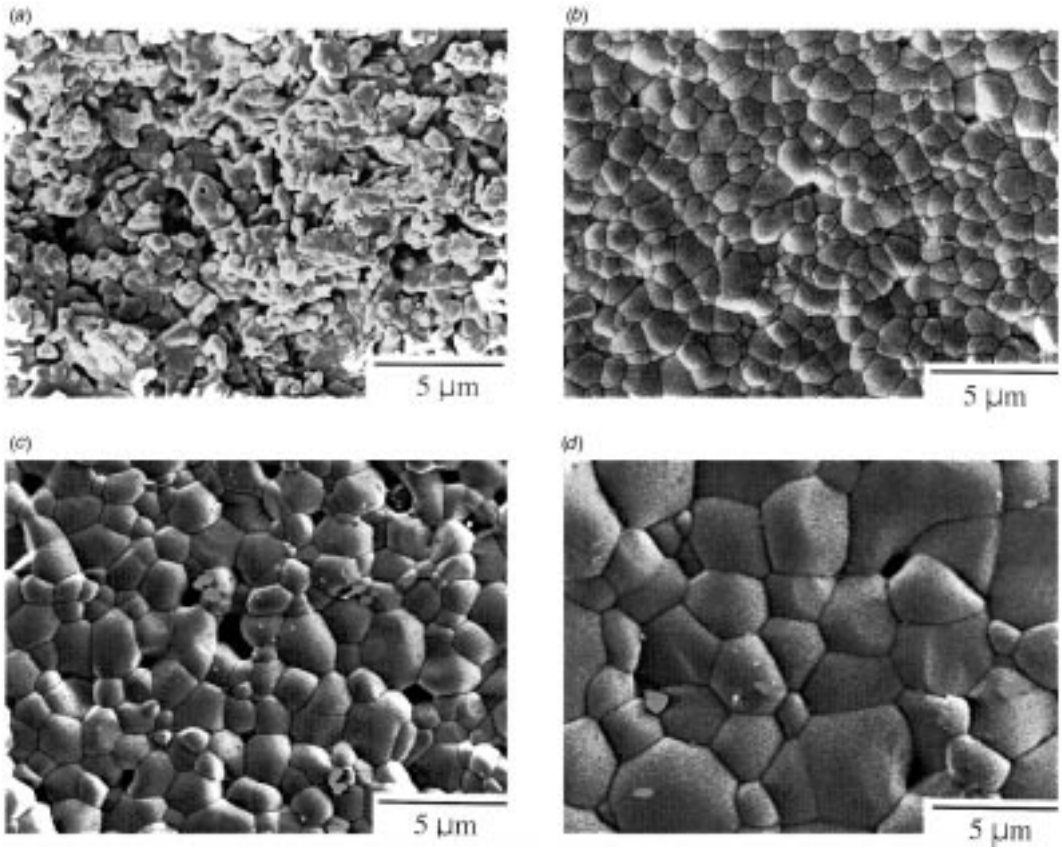

Fig. 10 Scanning electron micrographs of sintered surface. Sintering temperature: (*a*) 1200 °C, (*b*) 1300 °C, (*c*) 1400 °C, (*d*) 1500 °C.

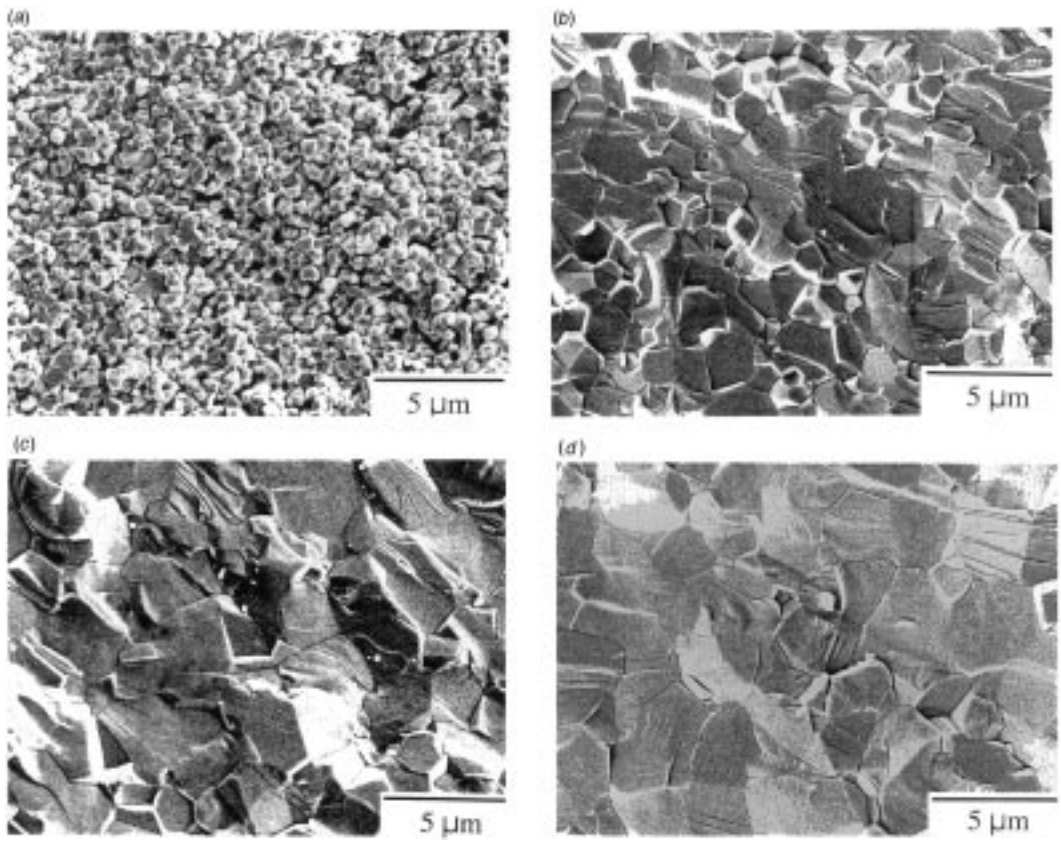

Fig. 11 Scanning electron micrographs of fracture surface of the sintered samples. Sintering temperature: (*a*) 1200 °C, (*b*) 1300 °C, (*c*) 1400 °C, (*d*) 1500 °C.

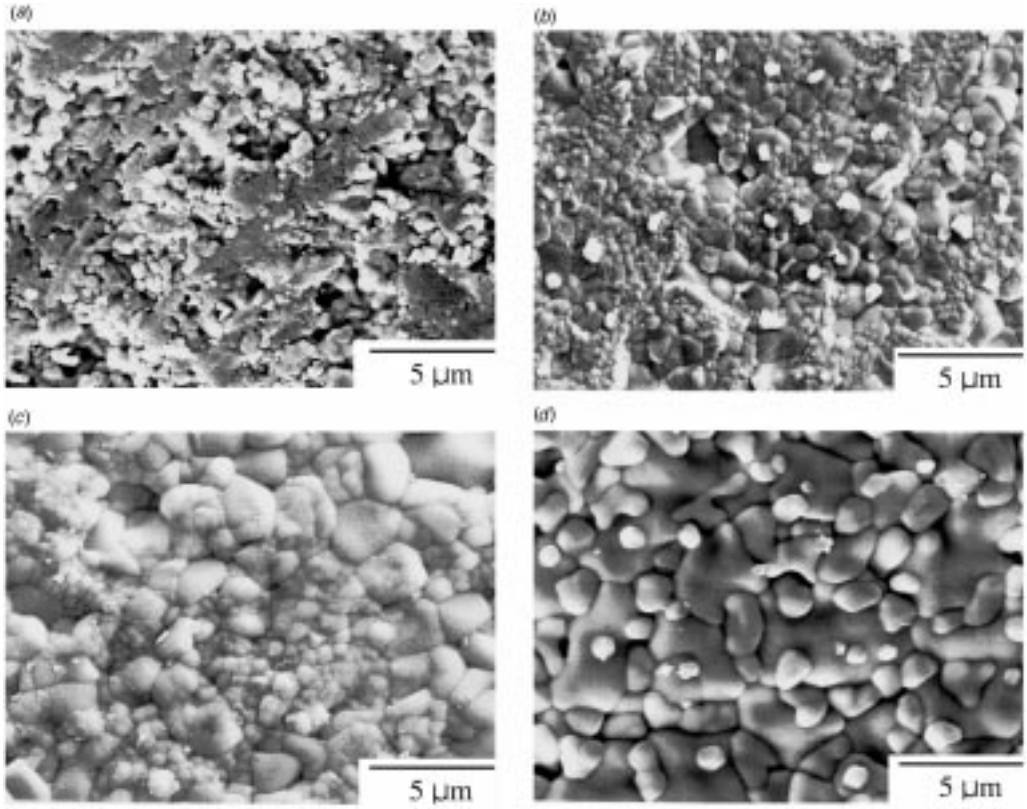

Fig. 12 Scanning electron micrographs of polished and thermally etched sintered samples. Sintering temperature: (*a*) 1200 °C, (*b*) 1300 °C, (*c*) 1400 °C, (*d*) 1500 °C.

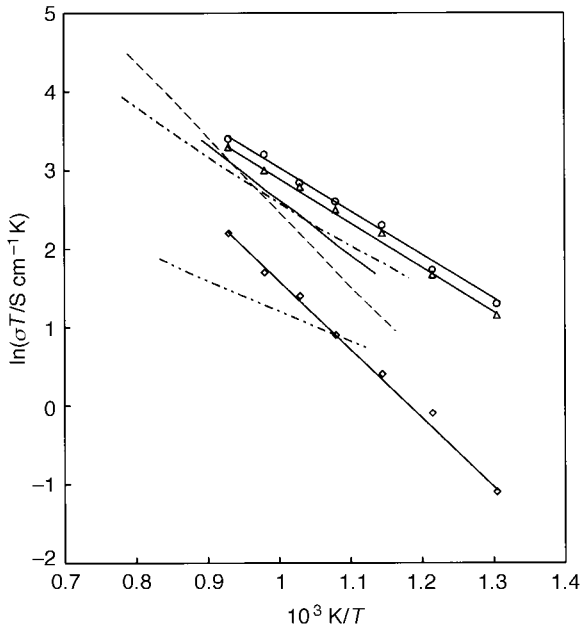

Fig. 13 Arrhenius plots of the electrical conductivities for Nd-doped $BaCeO_3$ ceramics in different atmospheres. From this work: ○, hydrogen; △, moist air; ◇, dry air. From previous studies: —, $BaCe_{0.9}Nd_{0.1}O_3$ in wet air (ref. 15); – – –, $BaCe_{0.9}Nd_{0.1}O_3$ in wet air (ref. 1); –·–, $BaCe_{0.9}Nd_{0.1}O_3$ in hydrogen (ref. 1); –··–, $BaCe_{0.95}Nd_{0.95}O_3$ in wet N_2 (ref. 14).

hydrogen atmosphere and 47.4 kJ mol^{-1} in moist air, while it is 70.8 kJ mol^{-1} in dry air. These differences are due to the fact that the material may demonstrate predominately oxygen ion conduction in dry air, so that the conductivity is low and the activation energy is high, while in hydrogen and moist air, proton conduction may predominate, leading to an increase in conductivity and a decrease in the activation energy. From Fig. 13 it can also be seen that in hydrogen and moist atmospheres, plots of $\ln(\sigma T)$ *vs.* $1/T$ obtained in the present work are more or less similar to those reported, but that the proton conductivity obtained in this work is higher than previously reported values. In this work, samples were prepared by a wet chemical process and homogeneous dense structures were obtained which may be favourable in terms of the electrical properties, while in the literature, samples were prepared by solid-state reaction methods. In this work, at 800 °C, a proton conductivity of 27 mS cm^{-1} was obtained in a hydrogen atmosphere, which makes this material a promising candidate as an electrolyte for moderate-temperature solid oxide fuel cells.

Conclusion

The formation of $BaCe_{0.9}Nd_{0.1}O_{3-\delta}$ perovskite phase from precipitated oxalate powders starts at 700 °C and is complete at 1000 °C. Ball-milling of the calcined powders in ethanol disperses possible agglomerates and consequently has a beneficial effect on the densification process. The calcination temperature had a major influence on the sintering process, and at 1100 °C, calcined powders possessed the highest sinterabilities. At a pressing pressure of >100 MPa, no apparent influence on the sintered density upon sintering at $\geqslant 1300$ °C was observed. When sintered at $T \geqslant 1300$ °C, a dense, homogeneous microstructure of the samples was obtained. Porosity remained at the grain boundaries and no exaggerated grain growth was produced. Nearly fully dense materials with 99.8% density could be obtained by optimizing the calcination and sintering processes. The proton conductivity of the samples prepared in this work is comparatively higher than those from traditional ceramic methods, which makes this material a promising candidate as an electrolyte for moderate-temperature solid oxide fuel cells.

This work was supported by the National Natural Science

Foundation of China. Fanglin Chen is grateful to Danish International Development Assistance (Danida) and State Science and Technology Commission (SSTC) of China for enabling his PhD study at the Materials Department, Risø National Laboratory. N. Bonanos is acknowledged for his constant interest and helpful advice in this work. Special thanks are given to P. Jensen and T. Strauss for their experimental assistance.

References

1 H. Iwahara, H. Uchida, K. Ono and K. Ogaki, *J. Electrochem. Soc*., 1988, **135**, 529.
2 H. Iwahara, H. Uchida and K. Morimoto, *J. Electrochem. Soc*., 1990, **137**, 462.
3 N. Bonanos, B. Ellis and M. Mahmood, *Solid State Ionics*, 1991, **44**, 305.
4 H. Iwahara, *Chem. Sens. Technol*., 1991, **3**, 117.
5 S. Hamakawa, T. Hibino and H. Iwahara, *J. Electrochem. Soc*., 1993, **140**, 459.
6 C. W. Tanner and A. V. Virkar, *J. Electrochem. Soc*., 1996, **143**, 1386.
7 H. Iwahara, T. Esaka, H. Uchida and N. Maeda, *Solid State Ionics*, 1981, **3/4**, 359.
8 N. Bonanos, B. Ellis, K. S. Knight and M. Mahmood, *Solid State Ionics*, 1989, **35**, 179.
9 M. H. Zhen and X. Chen, *Solid State Ionics*, 1994, **70/71**, 595.
10 E. M. Kelder, O. C. J. Nijs and J. Schoonman, *Solid State Ionics*, 1994, **68**, 5.
11 V. Agarwal and M. L. Liu, *J. Mater. Sci*., 1997, **32**, 619.
12 S. D. Flint and R. C. T. Slade, *Solid State Ionics*, 1995, **77**, 305.
13 B. A. Boukamp, *Solid State Ionics*, 1986, **18/19**, 136.
14 R. C. T. Slade and N. Singh, *Solid State Ionics*, 1991, **46**, 111.
15 D. A. Stevenson, N. Jiang, R. M. Buchanan and F. E. G. Henn, *Solid State Ionics*, 1993, **62**, 279.

Paper 6/08289K; *Received* 9*th December*, 1996